Research Article

Upconversion NaYF$_4$ Nanoparticles for Size Dependent Cell Imaging and Concentration Dependent Detection of Rhodamine B

Shigang Hu,[1] Xiaofeng Wu,[1] Zhijun Tang,[1] Zaifang Xi,[1] Zenghui Chen,[2] Pan Hu,[1] Yi Yu,[1] Huanyuan Yan,[3] and Yunxin Liu[2]

[1]*School of Information and Electrical Engineering, Hunan University of Science and Technology, Xiangtan 411201, China*
[2]*Department of Physics and Electronic Science, Hunan University of Science and Technology, Xiangtan 411201, China*
[3]*College of Mechanical and Electrical Engineering, Hunan University of Science and Technology, Xiangtan 411201, China*

Correspondence should be addressed to Yunxin Liu; lyunxin@163.com

Upconversion nanoparticles (UCNPs) based on NaYF$_4$ nanocrystals with strong upconversion luminescence are synthesized by the solvothermal method. The emission color of these NaYF$_4$ upconversion nanoparticles can be easily modulated by the doping. These NaYF$_4$ upconversion nanocrystals can be employed as fluorescence donors to pump fluorescent organic molecules. For example, the efficient luminescence resonant energy transfer (LRET) can be achieved by controlling the distance between NaYF$_4$:Yb^{3+}/Er^{3+} UCNPs and Rhodamine B (RB). NaYF$_4$:Yb^{3+}/Er^{3+} UCNPs can emit green light at the wavelength of ~540 nm while RB can efficiently absorb the green light of ~540 nm to emit red light of 610 nm. The LRET efficiency is highly dependent on the concentration of NaYF$_4$ upconversion fluorescent donors. For the fixed concentration of 3.2 μg/mL RB, the optimal concentration of NaYF$_4$:Yb^{3+}/Er^{3+} UCNPs is equal to 4 mg/mL which generates the highest LRET signal ratio. In addition, it is addressed that the upconversion nanoparticles with diameter of 200 nm are suitable for imaging the cells larger than 10 μm with clear differentiation between cell walls and cytoplasm.

1. Introduction

Upconversion luminescence (UCL) is a nonlinear, anti-Stokes process, whereby low-energy photons are converted to higher energy photons [1–3]. Compared to organic fluorophores and quantum dots, upconversion nanophosphors (UCNPs) exhibit high photochemical stability, sharp emission bandwidths, and large anti-Stokes shifts [4–6]. Lanthanide-doped UCNPs can be considered as dilute guest-host systems, where trivalent lanthanide ions are dispersed as guests in an appropriate inorganic host lattice with dimensions of less than 100 nm [7]. Light upconverting nanostructures employing lanthanide ions constitute an emerging research field recognized with wide ramifications and impact in many areas ranging from healthcare to energy and to security [8–12].

In the past few decades, lanthanide-based UCNPs have been regarded as a new generation of bioprobes for photoluminescent bioimaging applications [13]. UCL imaging for cells and animal tissues has attracted substantial attention because of the unique characteristics of upconversion materials, which can minimize the background interference from the autofluorescence of biosamples and enhance tissue penetration [14, 15]. Recently, upconversion nanocrystals with surface modification have been used for HeLa cell microscopic imaging in vitro [16] but rarely been developed for imaging other cells or tissues, especially for the in vivo imaging.

Fluorescence resonance energy transfer (FRET) is an optical process in which the energy is transferred from a donor at its excited state to a nearby ground-state acceptor [17, 18]. Efficient FRET process requires the donor and acceptor molecules in very close proximity and the donor emission spectrum to overlap with the acceptor absorption. Fluorescence resonance energy transfer (FRET) has been

widely used as a spectroscopic technique in various areas such as structural elucidation of biological molecules and their interactions, in vitro assays, in vivo monitoring in cellular research, nucleic acid analysis, signal transduction, light harvesting, and metallic nanomaterials [19–21]. When UCNPs are used as the energy donor, the upconversion luminescence upon NIR excitation of UCNPs is transferred to donor molecules, a mechanism named as luminescence resonance energy transfer (LRET) similar to FRET [22–24]. To date, several upconversion LRET (UC-LRET) nanosystems have been developed for detection of biomacromolecules (such as DNA [25], metalloproteinase [26], avidin [27], and thrombin [28]), metal cations, anions, and oxygen [29], in which the energy transfer process is utilized to modulate the UCL intensity.

In this work, a series of high-quality $NaYF_4$ UCNPs were synthesized by a facile solvent-thermal method. We focus on application of the multicolor upconversion nanoparticles in cells imaging and detection of Rhodamine B. On the other hand, we developed an upconversion LRET-based nanosystem composed of UCNPs and organic dyes (UCNPs@dye). The LRET-based UCNPs@dye systems can be extended for detecting other organic dyes and fluorescent proteins in living beings in vivo.

2. Experimental

Yttrium oxide (99.99%), ytterbium oxide (99.99%), erbium oxide (99.9%), and thulium oxide (99.99%) were purchased from Sinopharm Chemical Reagent Co., Ltd. 1-Octadecene (ODE) (90%) and oleic acid (OA) (90%) were purchased from Alfa Aesar (China) Chemical Co., Ltd. Sodium fluorescein (95%) and Rhodamine B (95%) were purchased from Sinopharm Chemical Reagent Co., Ltd. Rare earth chloride $RE(Cl)_3$ (RE Y, Yb, Er, and Tm) was prepared by dissolving the corresponding rare earth oxides in hydrochloric acid at a high temperature of 90°C. All other chemicals were of analytical grade and used without further purification.

2.1. Synthesis of $NaYF_4$ Nanoparticles.
In a typical procedure for the synthesis of $NaYF_4:Yb^{3+}$, Er^{3+}/Tm^{3+} nanoparticles, 2 mL water solution of $RECl_3 \cdot 6H_2O$ (0.4 M, RE = Lu, Yb, and Er/Tm) was added to a 50 mL flask containing ODE (12 mL) and OA (4 mL). The resulting mixture was heated to 160°C with constant stirring to remove residual water and oxygen. After 30 min, the temperature was reduced to room temperature with general flow of argon gas through the reaction flask. Shortly thereafter, 5 mL methanol solution of NH_4F (1.5 mmol) and NaOH (1 mmol) was added and the resultant solution was stirred for another 30 min under 50°C of temperature. After the methanol from the reaction mixture was evaporated, the solution was heated to 315°C under an argon atmosphere for 60 min and then cooled down to room temperature naturally. The resulting nanoparticles were precipitated by addition of ethanol, collected by centrifugation at 10000 rpm for 5 min, and washed with ethanol three times; finally these prepared nanocrystals could be redispersed in nonpolar organic solvent such as cyclohexane.

2.2. Characterization.
The size and morphology of the prepared nanoparticles were measured using H-7650c transmission electron microscopy (TEM) operating at 80 kV and JEM 3010 high-resolution transmission electron microscopy (HR-TEM) operating at 200 kV. The photoluminescence (PL) emission spectra were measured using a Hitachi F-2700 spectrophotometer equipped with a 980 nm laser as the excitation source. The photos of upconversion luminescence were digitally obtained by a Sony multiple CCD camera.

Imaging plant cells and animal issues incubated with upconversion nanoparticles were imaged using Olympus BX43 fluorescence microscopy under the excitation of a NIR 980 nm laser. The power density was equal to 100 mW/cm^2. The multicolor fluorescence was collected by a Tucsen H-694CICE digital camera. All studies were carried out at room temperature.

3. Results and Discussion

3.1. Upconversion Fluorescence Properties of $NaYF_4$ Nanoparticles.
To reveal the phase and size control, $NaYF_4$ nanocrystals with the doping of Yb^{3+}/Er^{3+} or Yb^{3+}/Tm^{3+} ionic pairs synthesized by the solvothermal method were characterized by TEM and high-resolution TEM (HR-TEM). It can be observed from Figure 1 that $NaYF_4:18\%Yb^{3+}/2\%Er^{3+}$ nanoparticles have an average diameter of 200 nm, typical hexagonal crystal facets, and good crystallinity. These uniform nanoparticles display regular morphology and high crystal quality. Typical high-resolution transmission electron microscopy (Figure 1(b)) shows the distance between the lattice fringes to be 0.32 nm along (0001) orientation in the $NaYF_4$ nanocrystals, which also revealed their highly crystalline nature and structural uniformity. If substituting the Er^{3+} (2 mol%) doping with Tm^{3+} ion (0.5 mol%), the average diameter of synthesized $NaYF_4$ nanoparticles particles reaches up to 300 nm.

The upconversion fluorescent spectra of $NaYF_4:18\%Yb^{3+}/2\%Er^{3+}$ and $NaYF_4:20\%Yb^{3+}/0.5\%Tm^{3+}$ nanocrystals in cyclohexane solution under the 980 nm laser excitation at different pump power are shown in Figures 2(a) and 2(c), respectively. The emission bands can easily be assigned to transition within the 4f-4f levels of the Er^{3+} and Tm^{3+} ions. The spectrum of the $NaYF_4:18\%Yb^{3+}/2\%Er^{3+}$ sample (Figure 2(a)) exhibits three distinct Er^{3+} emission bands. The three sharp emissions bands centered at 405 nm, 540 nm, and 656 nm were assigned to the Er^{3+}-$4f^n$ electronic transitions $^2H_{9/2} \rightarrow {}^4I_{15/2}$, $^4S_{3/2} \rightarrow {}^4I_{15/2}$, and $^4F_{9/2} \rightarrow {}^4I_{15/2}$. The total luminescence appears green in color due to a combination of green and red emissions from the Er^{3+} ion. $NaYF_4:20\%Yb^{3+}/0.5\%Tm^{3+}$ nanocrystals can emit intense blue light under the excitation of infrared light with wavelength of 980 nm. The corresponding upconversion fluorescent spectrum (Figure 2(c)) shows the main emission band centered at 472 nm which is ascribed to the 4f-shell electronic transition $^1G_4 \rightarrow {}^3H_6$ of Tm^{3+} ions. Upconverted emission was also detected in the red and ultraviolet (UV) regions of the spectrum and assigned to the $^1G_4 \rightarrow {}^3F_4$ (centered at 645 nm) and $^1D_2 \rightarrow {}^3H_6$ (centered at 355 nm) transitions,
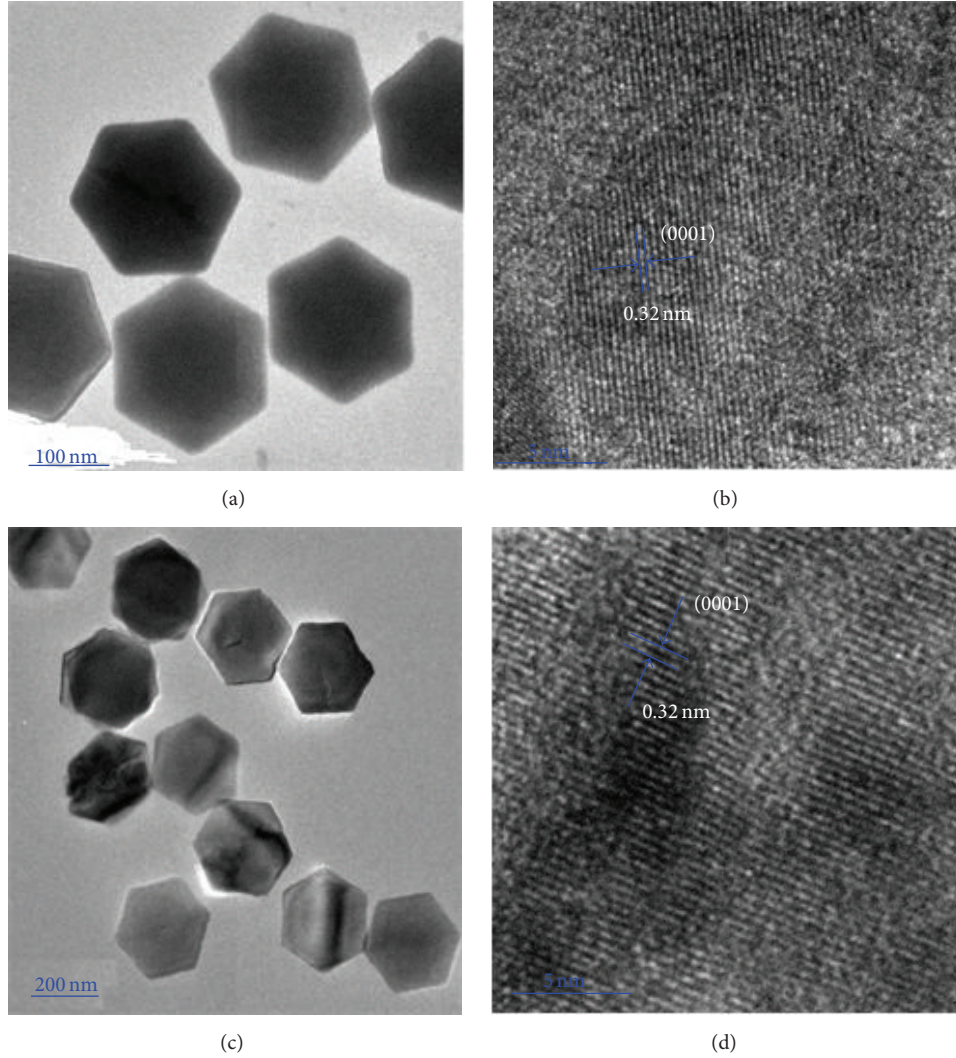
FIGURE 1: (a) TEM images of NaYF$_4$:18%Yb^{3+}/2%Er^{3+} nanocrystals; (b) the corresponding high-resolution TEM images (HR-TEM) of NaYF$_4$:18%Yb^{3+}/2%Er^{3+} nanocrystals. (c) TEM images of NaYF$_4$:20%Yb^{3+}/0.5%Tm^{3+} nanocrystals; (d) the corresponding high-resolution TEM images (HR-TEM) of NaYF$_4$:20%Yb^{3+}/0.5%Tm^{3+} nanocrystals.

respectively. The upconversion excitation pathways of the Er^{3+}/Yb^{3+} and Tm^{3+}/Yb^{3+} ion couples in these materials are well known and shown in Figure 3.

To better understand the populating mechanism of the excited states following near-infrared irradiation, the upconversion luminescence intensities versus the excitation power density are measured. It is known that, for unsaturated UC processes, the number of excitation photons which are required to generate an emission photon can be obtained by the following relation [30, 31]:

$$I_f \propto P^n, \tag{1}$$

where I_f is the fluorescent intensity, P is the pump laser power, and n is the number of the laser photons required. The excitation power dependence of the three emission bands of NaYF$_4$:18%Yb^{3+}/2%Er^{3+} nanocrystals is measured and treated by Auzel's method (Figure 2(b)) [32]. It should also be noted that the observed slope values, which correspond to the

number of photons required to generate an emission photon in the upconversion process, deviate from the expected values. For NaYF$_4$:18%Yb^{3+}/2%Er^{3+} nanocrystals, the n values are equal to 1.92 for the green emission and 1.87 for red emission, respectively. This indicates that two photons are involved in the upconversion process of both red and green emissions. The slope values of weak blue emission are equal to 2.81 which indicates a three-photon upconversion process. Figure 4 shows the excitation power dependence of the three emission bands of NaYF$_4$:20%Yb^{3+}/0.5%Tm^{3+} nanocrystals. The n values of blue emission equal 1.88, while those of red emission equal 1.93. The n values of both blue and red bands are much lower than the theoretical value ($n = 3$) that could be strongly ascribed to the saturation effect [33–35]. As the excited level $^3F_4$ has nearly saturated population, it will play a role of electron reservoir similar to the ground state and presents a false image for the electrons in the $^3F_4$ level that they transit from ground state to the upper ones. As a result,
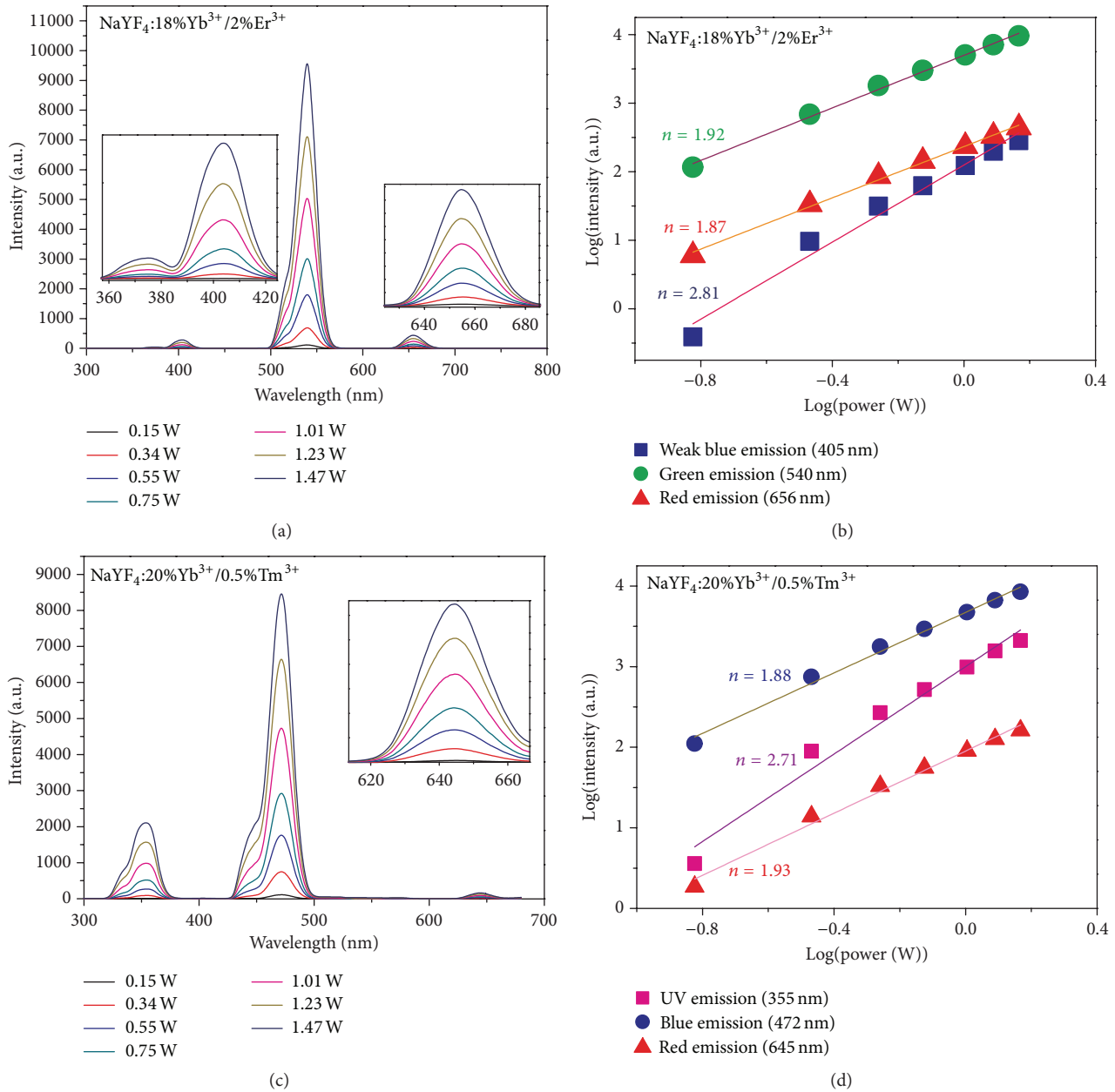
(a)

(b)

(c)

(d)

FIGURE 2: Power dependence of the upconversion emissions of $NaYF_4$ nanocrystals: (a) upconversion spectrum of $NaYF_4$:18%Yb^{3+}/2%Er^{3+} under different excitation power; (b) plots (log-log) of emission intensity versus excitation power in $NaYF_4$:Yb^{3+}/Er^{3+} nanocrystals; (c) upconversion spectrum of $NaYF_4$:20%Yb^{3+}/0.5%Tm^{3+} under different excitation power; (d) plots (log-log) of emission intensity versus excitation power in $NaYF_4$:Yb^{3+}/Tm^{3+} nanocrystals.

it is observed for blue and red emissions that the n value locates at the range of 1.0~2.0 which corresponds to a two-photon conversion process. This saturation phenomenon is also observed for the ultraviolet emission band which has the slope value of 2.71. It can be easily addressed that the saturation of $^3F_4$ level leads to the three-photon upconversion for $NaYF_4$:20%Yb^{3+}/0.5% nanocrystals.

To obtain the multicolor output from yellow-green to red emission in the visible region, the UC emissions of $NaYF_4$:Yb^{3+}, Er^{3+} nanocrystals are tuned by controlling the dopant concentration of the Yb^{3+} ion. In Figure 4, three

common emission peaks at 405 nm, 540 nm, and 656 nm are observed, which are assigned to the $^2H_{9/2} \rightarrow {}^4I_{15/2}$, $^4S_{3/2} \rightarrow {}^4I_{15/2}$, and $^4F_{9/2} \rightarrow {}^4I_{15/2}$ transition of Er^{3+}, respectively. Noticeably, the relative intensity of red to green emission gradually decreases along with the concentration of Yb^{3+} ions from 18 mol% to 80 mol%. With the increase of the concentration of Yb^{3+} ions, the color of $NaYF_4$:Yb^{3+}, Er^{3+} nanocrystals changes from green to yellow and then turns red (Figures 6(b)–6(e)).

The upconversion luminescence spectra of Yb^{3+}/Tm^{3+}/ Er^{3+} tridoped $NaYF_4$ nanoparticles were measured under a
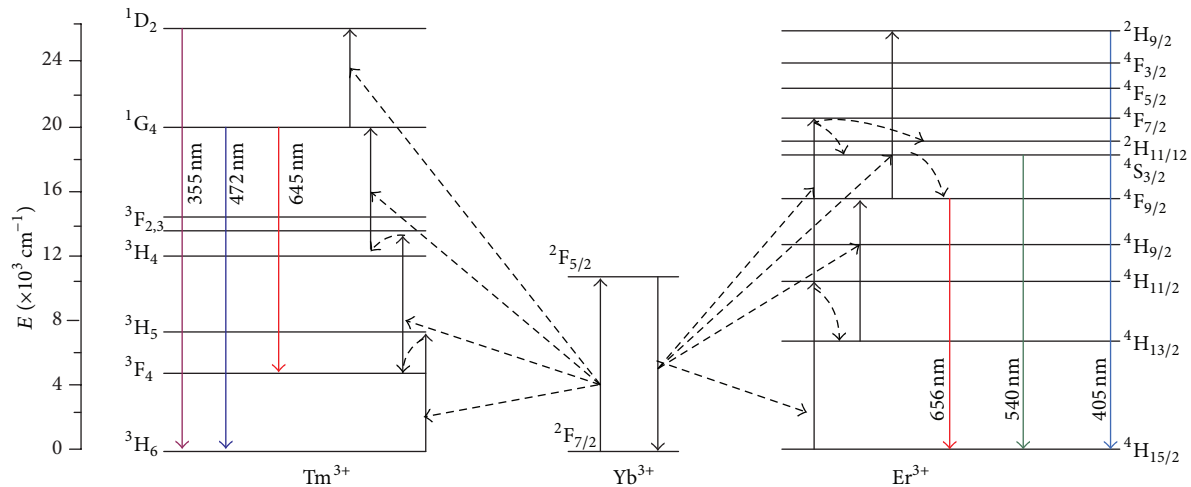
FIGURE 3: The energy level diagrams of the Er^{3+}, Tm^{3+}, and Yb^{3+} dopant ions and upconversion mechanisms following 980 nm laser diode excitation.
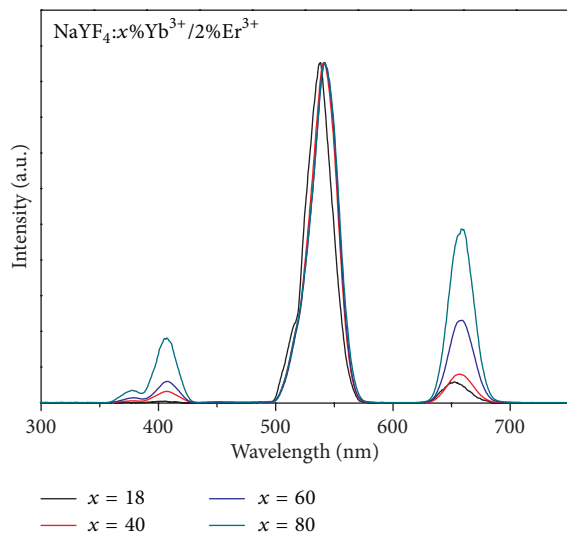

FIGURE 4: Room-temperature upconversion fluorescent spectra of $NaYF_4$ doped with (18, 40, 60, and 80%) Yb^{3+}/2%Er^{3+} under the excitation of a 980 nm laser diode at low pump power of 0.2 W.

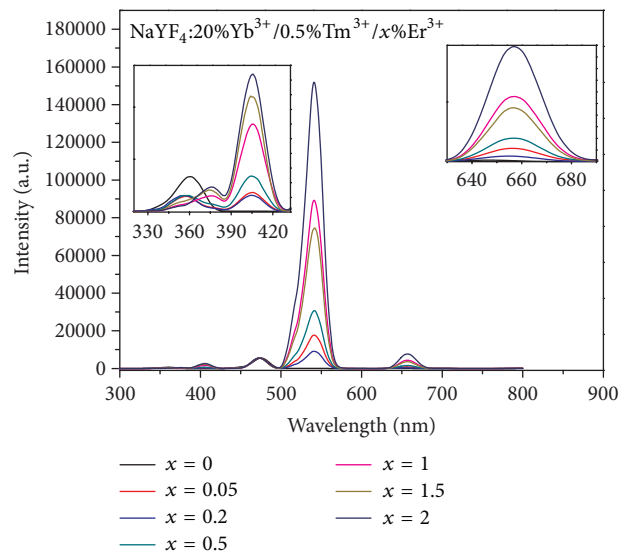FIGURE 5: The upconversion luminescence spectra of Yb^{3+}/Tm^{3+}/Er^{3+} tridoped $NaYF_4$ nanoparticles.

980 nm diode laser excitation and shown in Figure 5. For Yb^{3+}/Tm^{3+}/Er^{3+} tridoped $NaYF_4$ nanoparticles (Figure 5), the green emission peak at 540 nm is attributed to the $^4S_{3/2} \rightarrow {}^4I_{15/2}$ transition of Er^{3+}, while the blue emission peaks at 472 nm and 541 nm are attributed to the $^1G_4 \rightarrow {}^3H_6$ transition of Tm^{3+} ions. At the same time, the red, weak violet, and ultraviolet emission peaks can still be observed. It is quite clear from Figure 5 that the intensity ratio of the green to red (IRGR) emission varies with the change of the content of Er^{3+} ions. When the content of Er^{3+} ions is 2%, the IRGR reaches a maximum value. The color of $NaYF_4$:Yb^{3+}, Tm^{3+}, and Er^{3+} nanocrystals changes from cyan to green (Figures 6(g)–6(i)).

3.2. Cell Imaging. Bioimaging is an important diagnostic tool for researching biological phenomena in/between cells.

Conventional bioslice imaging technology has been gradually substituted by fluorescent imaging in biological and clinical application due to its defects of complicated slicing process and strictly limited thickness, which is incapable of imaging the cells in vivo. UCNP-based UC luminescence imaging shows excellent optical features, such as narrow anti-Stokes shifted light and low autofluorescence background. Because fluorescence-based techniques are inherently sensitive, selective, convenient, diverse, nondestructive, potentially real-time, and in situ, they have been widely used in biological imaging.

Here, the tomato skin cells were used for upconversion fluorescence imaging technique. In order to conveniently compare conventional bioslice imaging with upconversion fluorescent imaging, the slices of tomato skin were adopted as research objectives. However, it should be noted that
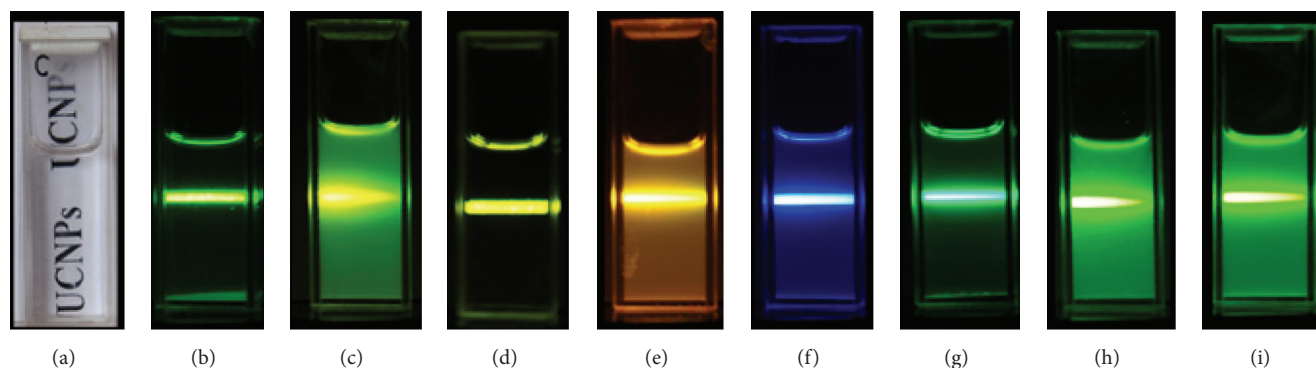
(a)   (b)   (c)   (d)   (e)   (f)   (g)   (h)   (i)

FIGURE 6: (a) Bright-field photo of the prepared $NaYF_4$ nanocrystals dispersed in cyclohexane. Eye-visible luminescence photos of the colloidal solution of $NaYF_4$ doped with (b–e) (18, 40, 60, 80)%Yb^{3+}/2%Er^{3+}; (f) 20%Yb^{3+}/0.5%Tm^{3+}; (g–i) 20%Yb^{3+}/0.5%Tm^{3+}/(0.05, 1, 2)%Er^{3+} under the excitation of a 980 nm laser diode.

the tomato skin without slicing process can be directly used for fluorescence imaging in vivo in practical biological applications.

The upconversion fluorescent bioimaging is detected in two kinds of cells incubated with multicolor $NaYF_4$ nanocrystals. First, the slices were dried at temperature of 35°C for one day. Second, an aqueous dispersion of UCNPs was added to container with these slices, which were incubated for 15 min at the temperature of 26°C. For cell and imaging, these hydrophobic upconversion $NaYF_4$ nanoparticles were transferred to be biocompatible and hydrophilic by coating them with PEG. The cell imaging was measured by confocal fluorescence microscopy (Olympus BX43) equipped with a 980 nm NIR diode laser after incubation in different kinds of $NaYF_4$ nanocrystal aqueous solution.

The fluorescent images of the tomato skin cells with upconversion $NaYF_4$:Yb^{3+}/Er^{3+} and $NaYF_4$:Yb^{3+}/Tm^{3+} nanoprobes are shown in Figure 7 for comparing with conventional slicing imaging. To change the multicolor upconversion nanoprobes, the imaging with green, blue, cyan, yellow, and red color could be obtained. It is clear from Figures 7(a)–7(c) that the tomato skin cells with an average size of 10 μm can be clear imaged by these 200 nm upconversion nanoprobes with remarkable differentiation between cell walls and cytoplasm. In addition, unambiguous cell structure is observed in the dark field with the assistance of UC fluorescence, which shows the possibility for the imaging in vivo. The shape and position of the cells overlapped very well in bright field and dark field, which indicated well biocompatibility between $NaYF_4$ nanocrystals and tomato skin cells. However, it can be seen from Figures 7(d) and 7(e) that these upconversion nanoprobes with diameter of 200 nm are not suitable for clearly imaging the cells with diameter smaller than 4 μm, in which the cell walls and cytoplasm can not be clearly differentiated. Conventional transmission imaging (left column in Figure 7) and upconversion fluorescent imaging (right column in Figure 7) are both capable of presenting the microstructure of slicing cells in vitro. However, the conventional slicing transmission imaging is incapable of presenting the cell microstructures in vivo.

3.3. Detection of Rhodamine B.

Rhodamine B (RB) is an efficient fluorescent dye which can emit red light of ~610 nm under the excitation of 540 nm green light and has well solubility in water, methanol, and ethanol. It is commonly used for dyeing textiles, paper, soap, leather, and even food in some countries. But the recent investigation indicates that the dye of RB may threaten the health of human beings. So it is urgent to develop a novel and efficient way for detecting the RB in the food.

There is a perfect overlap between the excitation spectra of Rhodamine B and the emission spectra of $NaYF_4$:Yb^{3+}, Er^{3+} nanoparticles in green region, so that an LRET-based sensor system can be successfully constructed by combining the UCNPs with Rhodamine B, in which UCNPs play a role of energy donor while Rhodamine B plays a role of energy acceptor. The synthesized UCNPs have an acidic ligand (oleic acid) which can quickly capture the basic molecule RB to form a close nanosystem of UCNPs@dye. In practical experiment, we control the distance between UCNPs and the fluorescent dyes by tuning the thickness of acidic ligand to obtain the optimal energy transfer efficiency in UCNPs@dye system. By comparing the relative emission intensities of red emission (RB) and green emission (UCNPs with emitter Er^{3+}), the concentration of RB can be correspondingly addressed.

Here, we used LRET tuned UCNPs for imaging tail fin tissues of crucian carp. The fluorescence imaging of tail fin tissues with UCNP1@RB under different excitation power is depicted in Figure 8, where the concentration of RB is fixed at 160 μg/mL. It is clearly observed that the tail fin tissues exhibited bright green light and yellow light to the naked eyes. As the excitation power increases, the yellow emission is becoming stronger and stronger. This indicates that the resonance energy transfer from UCNP to RB is enhanced with the increasing of excitation power. The increasing of excitation power makes the emission of UCNP stronger, which makes many more RB molecules be able to obtain the resonance energy and emit bright yellow light.

The UC luminescence spectra of UCNP@RB system with various concentrations of RB are shown in Figure 9. While the concentration of RB increases, the intensity of green
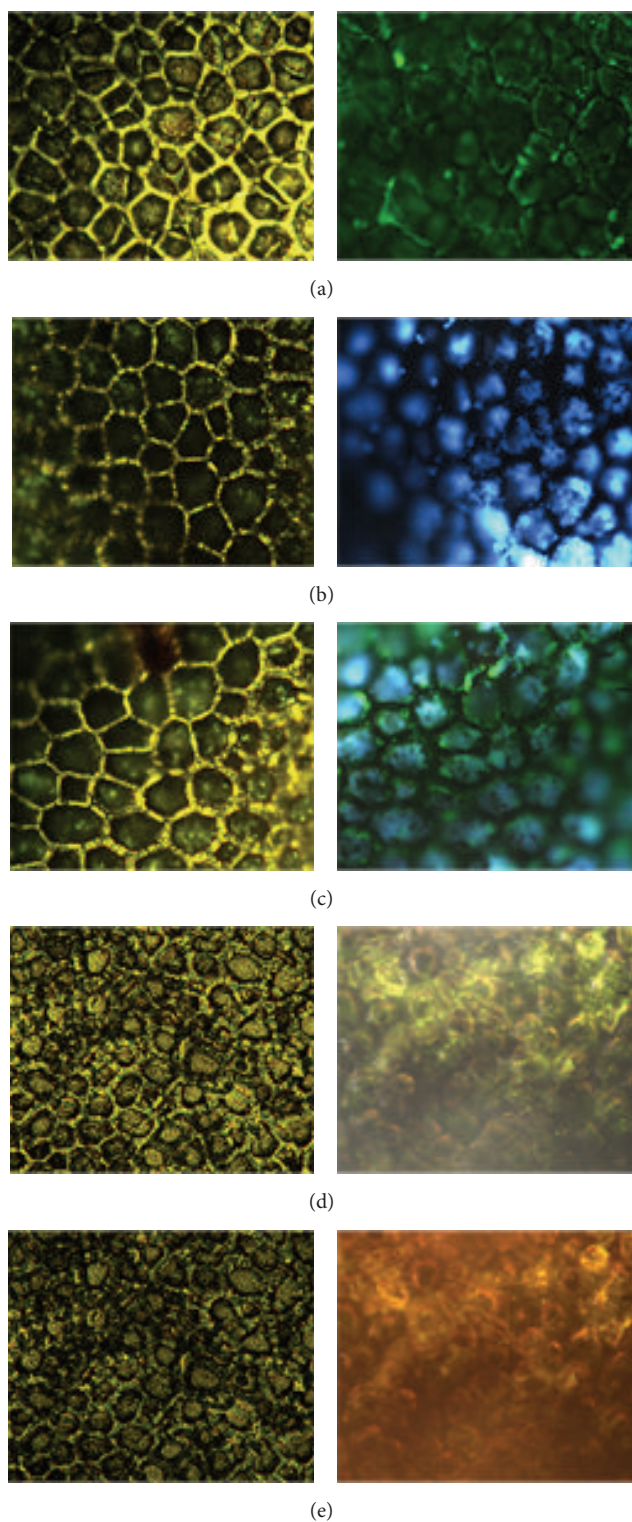
(a)

(b)

(c)

(d)

(e)

FIGURE 7: Right column: fluorescence microscope imaging of cells: (a) the skin issues loaded with $18\%Yb^{3+}/2\%Er^{3+}$; (b) the tomato skin cells loaded with $40\%Yb^{3+}/2\%Er^{3+}$; (c) the tomato skin cells loaded with $80\%Yb^{3+}/2\%Er^{3+}$; (d) the tomato skin cells loaded with $20\%Yb^{3+}/0.5\%Tm^{3+}$; and (e) the tomato skin cells with $NaYF_4:18\%Yb^{3+}/2\%Er^{3+}$ and $NaYF_4:20\%Yb^{3+}/0.5\%Tm^{3+}$. Left column: conventional slice transmission imaging.
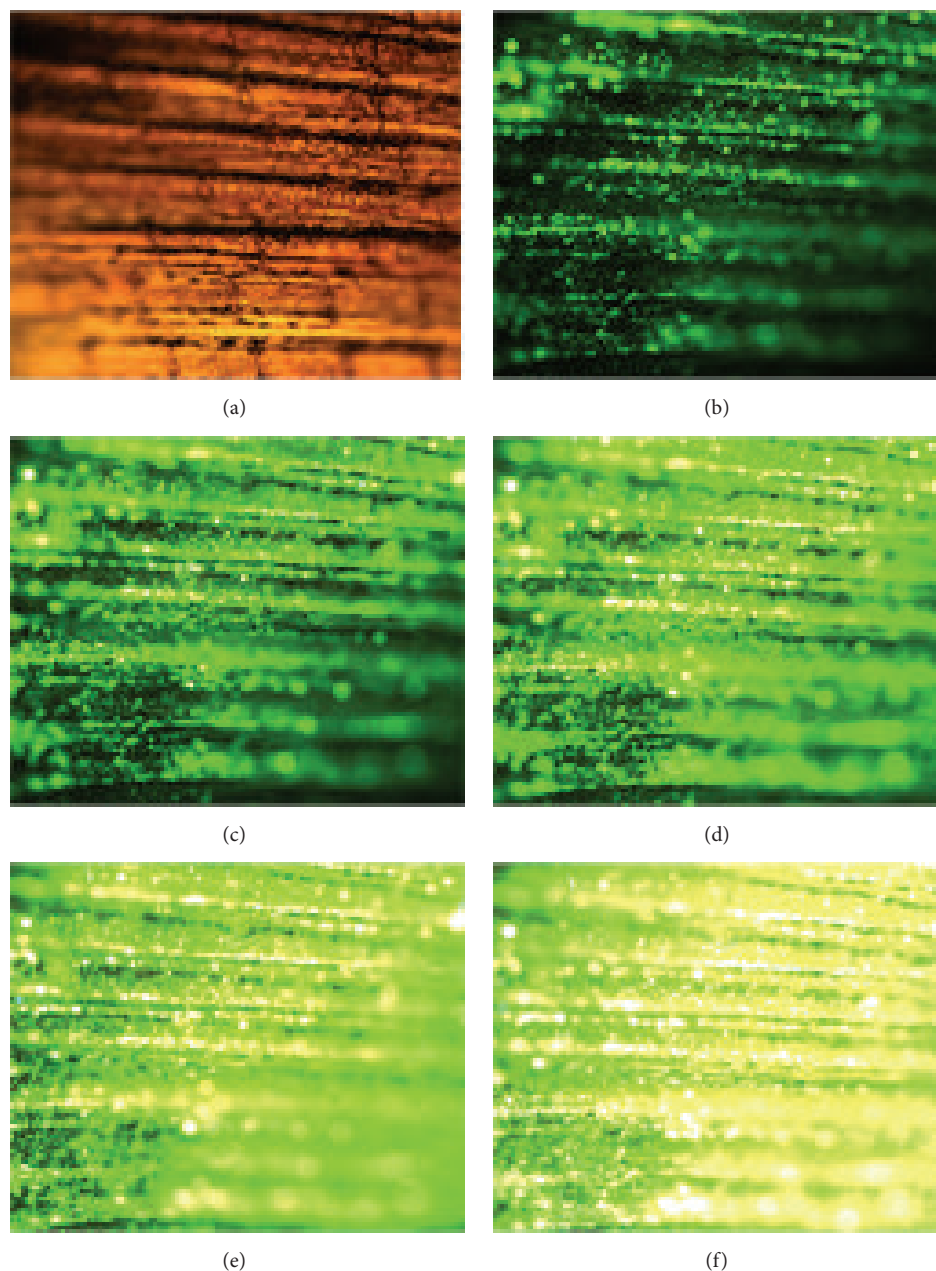
(a)

(b)

(c)

(d)

(e)

(f)

FIGURE 8: (a) Conventional slice transmission imaging, (b–f) fluorescence imaging of tail fin tissues of crucian carp with UCNP1@RhB under different excitation power: (b) 0.15 W, (c) 0.2 W, (d) 0.3 W, (e) 0.34 W, and (f) 0.55 W.

UCL peak decreases gradually, whereas the emissions at the range of 570~630 nm from RB occur via the resonance energy transfer from UCNP to those dye acceptors. The red emissions of UCNP at 656 nm are not affected after loading of RB molecules since those organic dyes have no absorption at this wavelength. When the concentration of RB is increased to 160 μg/mL, the green emission peaks of UCNP almost disappear. In this case, the green emission of UCNP has been completely absorbed by RB for emitting the peak centered at 610 nm. Importantly, the integral intensity ratio of red to green emission (IIRRGE) varies with decreasing the concentration of RB solution. The concentration of RB can

be easily addressed according to IIRRGE signal. The IIRRGE values can be used for the quick and precise detection of RB concentration in vitro or in vivo. Employing a 980 nm diode infrared power source of 0.34 W mm^{-2}, the detection limit of RB can reach 0.016 μg/mL, if the concentration of upconversion nanoprobes is properly controlled.

Upconversion fluorescent spectra of UCNPs@RB with various concentrations of NaYF$_4$ nanoparticles are shown in Figure 10. When the concentration of RB is fixed at 3.2 μg/mL, four emission peaks, centered at 408 nm, 525 nm, 650 nm, and 590 nm, are observed for this UCNPs@RB system which can be assigned to the electronic transitions $^2H_{9/2}$-$^4I_{15/2}$,
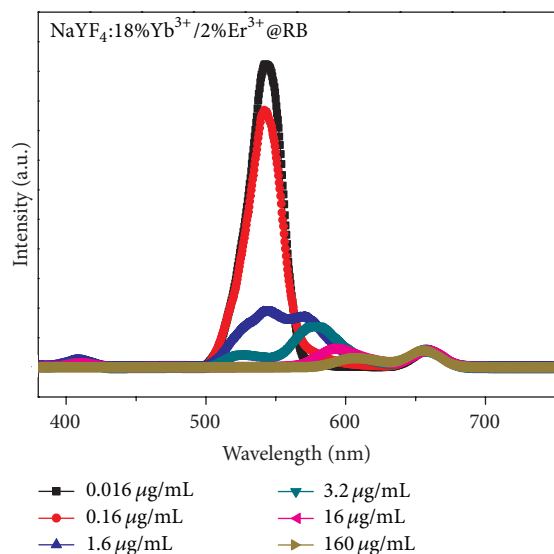
FIGURE 9: Evolution of the fluorescence of UCNP@RB with different concentration of RB under the excitation power of 0.34 W.
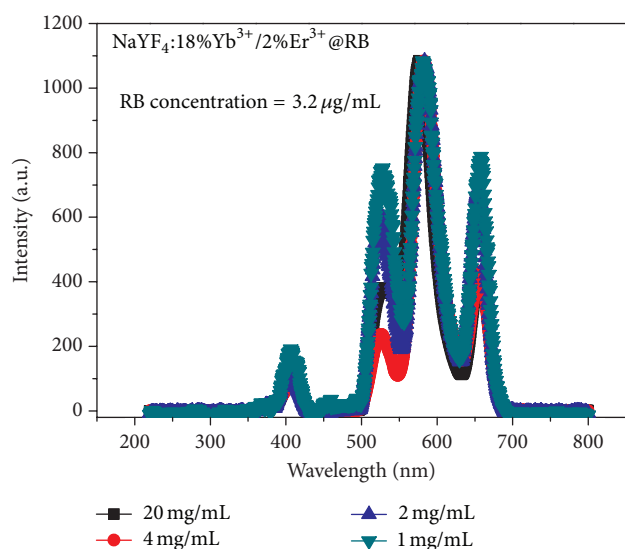

FIGURE 10: Evolution of the fluorescence spectra of UCNPs@RB in the presence of various concentrations of UCNPs (from 1 to 20 mg/mL).

$^2H_{11/2}$-$^4I_{15/2}$, and $^4F_{9/2}$-$^4I_{15/2}$ of Er^{3+} ions and the emission of RB, respectively. It is clear that the intensity ratio of RB emission peak to the green emission peak of Er^{3+} reaches to the highest value when the concentration of upconversion NaYF$_4$:Yb^{3+}, Er^{3+} fluorescent donors is equal to 4 mg/mL.

4. Conclusions

In conclusion, NaYF$_4$ upconversion fluorescent nanoprobes doped with Yb^{3+} and Er^{3+} or Tm^{3+} were successfully synthesized via the solvothermal method. Modulated UCL emission spectra were obtained via changing the doping. Fluorescent biological imaging for living beings can be achieved by using these multicolor NaYF$_4$ upconversion nanocrystals as fluorescent probes without the need of a slicing process. These NaYF$_4$ upconversion nanocrystals can be employed as fluorescence donors to pump fluorescent organic molecules. For example, the efficient luminescence resonant energy transfer (LRET) can be achieved by controlling the distance between NaYF$_4$:Yb^{3+}/Er^{3+} UCNPs and Rhodamine B (RB). NaYF$_4$:Yb^{3+}/Er^{3+} UCNPs can emit green light at the wavelength of ~540 nm while RB can efficiently absorb the green light of ~540 nm to emit red light of 610 nm. The LRET efficiency is highly dependent on the concentration of NaYF$_4$ upconversion fluorescent donors. For the fixed concentration of 3.2 μg/mL RB, the optimal concentration of NaYF$_4$:Yb^{3+}/Er^{3+} UCNPs is equal to 4 mg/mL which generates the highest LRET signal ratio. In addition, it is addressed that the upconversion nanoparticles with diameter of 200 nm are suitable for imaging the cells larger than 10 μm with clear differentiation between cell walls and cytoplasm.

Conflict of Interests

The authors declare that there is no conflict of interests regarding the publication of this paper.
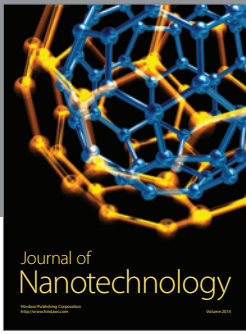
Acknowledgments

References

[1] J. De Wild, J. K. Rath, A. Meijerink, W. G. J. H. M. Van Sark, and R. E. I. Schropp, "Enhanced near-infrared response of a-Si:H solar cells with β-NaYF$_4$:Yb^{3+} (18%), Er^{3+} (2%) upconversion phosphors," *Solar Energy Materials and Solar Cells*, vol. 94, no. 12, pp. 2395–2398, 2010.

[2] F. Wang, D. Banerjee, Y. Liu, X. Chen, and X. Liu, "Upconversion nanoparticles in biological labeling, imaging, and therapy," *Analyst*, vol. 135, no. 8, pp. 1839–1854, 2010.

[3] C. Wang, H. Tao, L. Cheng, and Z. Liu, "Near-infrared light induced in vivo photodynamic therapy of cancer based on upconversion nanoparticles," *Biomaterials*, vol. 32, no. 26, pp. 6145–6154, 2011.

[4] Q. Liu, Y. Sun, T. Yang, W. Feng, C. Li, and F. Li, "Sub-10 nm hexagonal lanthanide-doped NaLuF$_4$ upconversion nanocrystals for sensitive bioimaging in vivo," *Journal of the American Chemical Society*, vol. 133, no. 43, pp. 17122–17125, 2011.

[5] F. Wang and X. Liu, "Multicolor tuning of lanthanide-doped nanoparticles by single wavelength excitation," *Accounts of Chemical Research*, vol. 47, no. 4, pp. 1378–1385, 2014.

[6] Z. Chen, X. Wu, S. Hu et al., "Multicolor upconversion NaLuF$_4$ fluorescent nanoprobe for plant cell imaging and detection of sodium fluorescein," *Journal of Materials Chemistry C*, vol. 3, no. 1, pp. 153–161, 2015.

[7] G. Chen, H. Ågren, T. Y. Ohulchanskyy, and P. N. Prasad, "Light upconverting core-shell nanostructures: nanophotonic control for emerging applications," *Chemical Society Reviews*, vol. 44, no. 6, pp. 1680–1713, 2015.

[8] F. Ai, Q. Ju, X. Zhang, X. Chen, F. Wang, and G. Zhu, "A core-shell-shell nanoplatform upconverting near-infrared light at 808 nm for luminescence imaging and photodynamic therapy of cancer," *Scientific Reports*, vol. 5, Article ID 10785, 2015.

[9] A. Gnach, T. Lipinski, A. Bednarkiewicz, J. Rybka, and J. A. Capobianco, "Upconverting nanoparticles: assessing the toxicity," *Chemical Society Reviews*, vol. 44, no. 6, pp. 1561–1584, 2015.

[10] Z. Li, T. Liang, S. Lv, Q. Zhuang, and Z. Liu, "A rationally designed upconversion nanoprobe for in vivo detection of hydroxyl radical," *Journal of the American Chemical Society*, vol. 137, no. 34, pp. 11179–11185, 2015.

[11] D. Peng, Q. Ju, X. Chen et al., "Lanthanide-doped energy cascade nanoparticles: full spectrum emission by single wavelength excitation," *Chemistry of Materials*, vol. 27, no. 8, pp. 3115–3120, 2015.

[12] X. Chen, Z. Zhao, M. Jiang, D. Que, S. Shi, and N. Zheng, "Preparation and photodynamic therapy application of NaYF$_4$: Yb, Tm–NaYF$_4$:Yb, Er multifunctional upconverting nanoparticles," *New Journal of Chemistry*, vol. 37, no. 6, pp. 1782–1788, 2013.

[13] G. Chen, T. Y. Ohulchanskyy, S. Liu et al., "Core/shell NaGdF$_4$: Nd^{3+}/NaGdF$_4$ nanocrystals with efficient near-infrared to near-infrared downconversion photoluminescence for bioimaging applications," *ACS Nano*, vol. 6, no. 4, pp. 2969–2977, 2012.

[14] J. Zhou, Z. Liu, and F. Li, "Upconversion nanophosphors for small-animal imaging," *Chemical Society Reviews*, vol. 41, no. 3, pp. 1323–1349, 2012.

[15] Q. Liu, W. Feng, T. Yang, T. Yi, and F. Li, "Upconversion luminescence imaging of cells and small animals," *Nature Protocols*, vol. 8, no. 10, pp. 2033–2044, 2013.

[16] M. Wang, C.-C. Mi, W.-X. Wang et al., "Immunolabeling and NIR-excited fluorescent imaging of HeLa cells by using NaYF$_4$:Yb, Er upconversion nanoparticles," *ACS Nano*, vol. 3, no. 6, pp. 1580–1586, 2009.

[17] R. B. Sekar and A. Periasamy, "Fluorescence resonance energy transfer (FRET) microscopy imaging of live cell protein localizations," *The Journal of Cell Biology*, vol. 160, no. 5, pp. 629–633, 2003.

[18] E. Oh, M.-Y. Hong, D. Lee, S.-H. Nam, H. C. Yoon, and H.-S. Kim, "Inhibition assay of biomolecules based on fluorescence resonance energy transfer (FRET) between quantum dots and gold nanoparticles," *Journal of the American Chemical Society*, vol. 127, no. 10, pp. 3270–3271, 2005.

[19] A. K. Kenworthy, "Imaging protein-protein interactions using fluorescence resonance energy transfer microscopy," *Methods*, vol. 24, no. 3, pp. 289–296, 2001.

[20] T. Ha, "Single-molecule fluorescence resonance energy transfer," *Methods*, vol. 25, no. 1, pp. 78–86, 2001.

[21] V. V. Didenko, "DNA probes using fluorescence resonance energy transfer (FRET): designs and applications," *BioTechniques*, vol. 31, no. 5, pp. 1106–1121, 2001.

[22] J. Zhang, C. Mi, H. Wu, H. Huang, C. Mao, and S. Xu, "Synthesis of NaYF$_4$: Yb/Er/Gd up-conversion luminescent nanoparticles and luminescence resonance energy transfer-based protein detection," *Analytical Biochemistry*, vol. 421, no. 2, pp. 673–679, 2012.

[23] L. Cheng, K. Yang, M. Shao, S.-T. Lee, and Z. Liu, "Multicolor in vivo imaging of upconversion nanoparticles with emissions tuned by luminescence resonance energy transfer," *The Journal of Physical Chemistry C*, vol. 115, no. 6, pp. 2686–2692, 2011.

[24] C. Mi, H. Gao, F. Li, and S. Xu, "Synthesis of surface amino-functionalized NaGdF$_4$:Ce,Tb nanoparticles and their luminescence resonance energy transfer (LRET) with Au nanoparticles," *Colloids and Surfaces A: Physicochemical and Engineering Aspects*, vol. 395, pp. 152–156, 2012.

[25] Y. Wang, Z. Wu, and Z. Liu, "Upconversion fluorescence resonance energy transfer biosensor with aromatic polymer nanospheres as the lable-free energy acceptor," *Analytical Chemistry*, vol. 85, no. 1, pp. 258–264, 2013.

[26] Y. Wang, P. Shen, C. Li, Y. Wang, and Z. Liu, "Upconversion fluorescence resonance energy transfer based biosensor for ultrasensitive detection of matrix metalloproteinase-2 in blood," *Analytical Chemistry*, vol. 84, no. 3, pp. 1466–1473, 2012.

[27] L. Wang, R. Yan, Z. Huo et al., "Fluorescence resonant energy transfer biosensor based on upconversion-luminescent nanoparticles," *Angewandte Chemie*, vol. 44, no. 37, pp. 6054–6057, 2005.

[28] H. Chen, F. Yuan, S. Wang, J. Xu, Y. Zhang, and L. Wang, "Aptamer-based sensing for thrombin in red region via fluorescence resonant energy transfer between NaYF$_4$: Yb, Er upconversion nanoparticles and gold nanorods," *Biosensors and Bioelectronics*, vol. 48, pp. 19–25, 2013.

[29] C. Zhang, Y. Yuan, S. Zhang, Y. Wang, and Z. Liu, "Biosensing platform based on fluorescence resonance energy transfer from upconverting nanocrystals to graphene oxide," *Angewandte Chemie International Edition*, vol. 50, no. 30, pp. 6851–6854, 2011.

[30] J. F. Suyver, A. Aebischer, S. García-Revilla, P. Gerner, and H. U. Güdel, "Anomalous power dependence of sensitized upconversion luminescence," *Physical Review B*, vol. 71, no. 12, Article ID 125123, 9 pages, 2005.

[31] M. Pollnau, D. R. Gamelin, S. R. Lüthi, H. U. Güdel, and M. P. Hehlen, "Power dependence of upconversion luminescence in lanthanide and transition-metal-ion systems," *Physical Review B: Condensed Matter and Materials Physics*, vol. 61, no. 5, pp. 3337–3346, 2000.

[32] F. E. Auzel, "Materials and devices using double-pumped-phosphors with energy transfer," *Proceedings of the IEEE*, vol. 61, no. 6, pp. 758–786, 1973.

[33] F. Pandozzi, F. Vetrone, J.-C. Boyer et al., "A spectroscopic analysis of blue and ultraviolet upconverted emissions from Gd$_3$Ga$_5$O$_{12}$:Tm^{3+}, Yb^{3+} nanocrystals," *Journal of Physical Chemistry B*, vol. 109, no. 37, pp. 17400–17405, 2005.

[34] H. Sun, Z. Duan, G. Zhou et al., "Structural and up-conversion luminescence properties in Tm^{3+}/Yb^{3+}-codoped heavy metal oxide–halide glasses," *Spectrochimica Acta A: Molecular and Biomolecular Spectroscopy*, vol. 63, no. 1, pp. 149–153, 2006.

[35] S. Xu, H. Ma, D. Fang, Z. Zhang, and Z. Jiang, "Upconversion luminescence and mechanisms in Yb^{3+}-sensitized Tm^{3+}-doped oxyhalide tellurite glasses," *Journal of Luminescence*, vol. 117, no. 2, pp. 135–140, 2006.